

# Elliptical Pipette Generated Large Microdroplets for POC Visual ddPCR Quantification of Low Viral Load

Liao Chen, Vivek Yadav, Chenguang Zhang, Xiaoye Huo, Ceming Wang, Satyajyoti Senapati, and Hsueh-Chia Chang\*



Cite This: <https://doi.org/10.1021/acs.analchem.1c00192>



Read Online

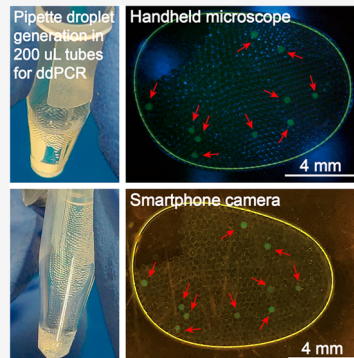
ACCESS |

Metrics & More

Article Recommendations

Supporting Information

**ABSTRACT:** Rapid point-of-care (POC) quantification of low virus RNA load would significantly reduce the turn-around time for the PCR test and help contain a fast-spreading epidemic. Herein, we report a droplet digital PCR (ddPCR) platform that can achieve this sensitivity and rapidity without bulky lab-bound equipment. The key technology is a flattened pipette tip with an elliptical cross-section, which extends a high aspect-ratio microfluidic chip design to pipette scale, for rapid (<5 min) generation of several thousand monodispersed droplets ~150 to 350  $\mu\text{m}$  in size with a CV of ~2.3%. A block copolymer surfactant (polyoxyalkylene F127) is used to stabilize these large droplets in oil during thermal cycling. At this droplet size and number, positive droplets can be counted by eye or imaged by a smartphone with appropriate illumination/filtering to accurately quantify up to 100 target copies. We demonstrate with 2019 nCoV-PCR assay LODs of 3.8 copies per 20  $\mu\text{L}$  of sample and a dynamic range of 4–100 copies. The ddPCR platform is shown to be inhibitor resistant with spiked saliva samples, suggesting RNA extraction may not be necessary. It represents a rapid 1.5-h POC quantitative PCR test that requires just a pipette equipped with elliptical pipette tip, a commercial portable thermal cycler, a smartphone, and a portable trans-illuminator, without bulky and expensive micropumps and optical detectors that prevent POC application.



## INTRODUCTION

Reverse transcription polymerase chain reaction (rt-PCR) remains the gold standard for SARS-CoV-2 virus detection from nasopharyngeal swabs and/or saliva samples. However, the need to conduct this assay in laboratories and the resulting long transport time have become a bottleneck on the control of a rapidly spreading pandemic with high positivity rates. Even with its expensive and lab-bound optical instruments, the false negative rate of rt-PCR detection especially for the newly infected samples with low viral concentration is not satisfactory.<sup>1–4</sup> It is known that, compared with rt-PCR, droplet digital polymerase chain reaction (ddPCR) has better sensitivity by partitioning the samples into large numbers of droplets to enrich the virus RNA and also mitigate the influences of PCR inhibitors.<sup>5–10</sup> Their simpler optical detectors also suggest ddPCR products can be used at the point-of-care (POC), without transportation to laboratories.

Nevertheless, a viable rapid POC ddPCR COVID screening test has yet to be reported. Alternatives to the bulky and expensive micropumps in commercial products have been proposed.<sup>11</sup> However, the main challenge for POC ddPCR is the droplet size and the related lab-bound optical detection platform. Commercial ddPCR products use carefully designed flow focusing (for example, products by BioRad) and step-emulsification (by Still) microfluidic chips typically generate droplets that are picoliters to several nanoliters in volume. The

current commercial RNA extraction kit yields about 1–100 copies of virus RNA from early stage patients in a typical 10  $\mu\text{L}$  extract for PCR tests.<sup>6,7</sup> Such low viral load is near the limit-of-detection of many PCR tests. Once the extract is combined with the PCR mixture, a total of 20–30  $\mu\text{L}$  will then need to be converted into droplets, corresponding to  $10^5$  to  $10^7$  droplets. The search for fewer than 100 positive droplets out of approximately one million droplets requires spreading a large monolayer of droplets if panned imaging is used<sup>12</sup> or a flow format with individual droplet interrogation.<sup>13</sup> Both are time-consuming, equipment-intensive, and error-prone, leading to sensitivity corruption even with the expensive and bulky optical detectors. They are not POC operations.

It is possible for some droplet generation technologies to generate larger and fewer droplets. However, large (>100  $\mu\text{m}$ ) droplets have thermal stabilization issues during PCR amplification, leading to inaccurate quantification.<sup>14–16</sup> There is also a detection issue with larger droplets. The fluorescence intensity of the PCR reporter is a function of the droplet size,

Received: January 14, 2021

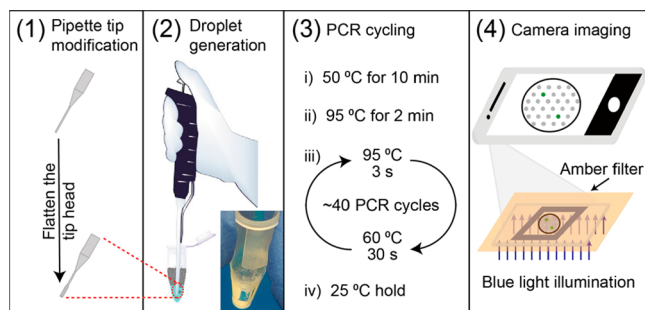
Accepted: April 9, 2021

as it is determined by the concentration of the reporter. Hence, for a typical 30 to 40-cycle assay, the activated number of reporters in a droplet must yield an overall concentration over one droplet that is higher than the threshold required by a particular detector. Ideally, with droplets that are larger than 100  $\mu\text{m}$ , a high enough fluorescence intensity may permit quantification by eye with blue light illumination (transilluminator) and imaging by a smartphone camera. Visual quantification would completely remove the need for expensive and bulky optical detectors and enable a rapid POC ddPCR test, if the bulky/expensive micropump is also eliminated.

What is required for a low viral-load POC ddPCR virus test is then an optimum droplet size and an optimum number of droplets. The droplets must be small enough so that the reporter fluorescent intensity is visible to the eye or a smartphone camera, to eliminate the lab-bound optical detectors. The droplets must yet be large enough ( $>100 \mu\text{m}$ ) so that all of the positive droplets can be easily discerned within one smartphone imaging frame. These large droplets must be stable during thermal cycling and should be easily generated without an expensive lab-bound commercial micropump. There must still be enough droplets so that there is only one molecule per positive droplet, as it would be difficult to quantify negative droplets without optical detectors. Hence, the balance between size and number stipulates that only low viral load samples can be quantified. The trade-off is then the high viral load of late-stage patients cannot be quantified, although their infection can still be sensitively diagnosed. However, viral load quantification is often unnecessary for late-stage patients and, if necessary for therapy management, can be measured with conventional PCR tests at the hospital or by diluting the sample.

Despite the multitude of constraints, we report here just such a low viral-load POC platform (see Scheme 1).

**Scheme 1. Low-Cost POC Droplet Digital PCR: (1) Fabrication of Head-Flattened Pipette Tips; (2) Uniform Large Microdroplets Generation with Pipette Tips; (3) Large Microdroplets Are Stabilized for PCR Thermal Cycling; (4) Detection of the Large Microdroplets by Eye or Smartphone with a Transilluminator**



Approximately  $\sim 1000$  to  $\sim 10\,000$  large microdroplets of optimal size (150 to 350  $\mu\text{m}$ ) are generated by head-flattened pipette tips in 5 min. The head-flattened pipette tip has an elliptic cross-section and is prewetted by oil. It is a pipette-tip/capillary version of an earlier design for a high-aspect ratio droplet-generating microfluidic chip.<sup>17</sup> The wetting oil film produces two long oil/water menisci at the sides of the pipette tip with a high curvature that is the same as the pipette tip wall. The high capillary pressure produced by these two side menisci control droplet pinching and produce monodispersed droplets.

In contrast to the longitudinal curvature (capillary pressure) that stabilizes pinching of the extruding jet into droplets, the side curvature (capillary pressure) actually drives the pinching. An axisymmetric interface hence pinches off with equal contribution from these two opposing capillary pressures and produces nonmonodispersed droplets with satellite droplets due to the competition. The interface with an elliptical cross section, however, favors the side capillary pressure that drives pinch off and hence produces monodispersed droplets, when the aspect ratio exceeds a critical value of 3.5.<sup>18</sup> The static capillary mechanism also ensures that the droplet generation is insensitive to the pipetting flow rate<sup>17–21</sup> and the droplet diameter is proportional to the width of the pipette tip orifice. Precise control of the flow rate is hence unnecessary, as in flow focusing and step emulsification. As a result, monodispersed large microdroplets are easily prepared by pipette guns equipped with head-flattened tips into standard 200  $\mu\text{L}$  PCR tubes loaded with fluorocarbon oil. The sample utilization is  $\sim 100\%$ , and the generated droplets in PCR tubes are immediately ready for thermal cycling.

These large droplets are not stable during PCR cycling and will coalesce. This thermal stability issue of large droplets is typically solved with a very high concentration of surfactants,<sup>22</sup> specially designed surfactants,<sup>23,24</sup> or cross-linking into gel beads.<sup>25</sup> Inspired by the versatile micelle formation and aggregation/patterning phenomena of the biocompatible polyoxyalkylene block copolymer F127 solution with respect to temperature changes,<sup>26–28</sup> we introduce this F127 solution into the aqueous phase ( $\geq 0.01$  w/v%) together with the limited amount of fluorosurfactant (1–2 wt %) in the oil phase to synergistically stabilize the large microdroplets for PCR cycling. We then demonstrate that the positive droplets are discernible by eye, after 30–40 cycles of PCR, with a filtered transilluminator. The detection limits are shown to be 3.8 (N target region) and 3.0 (ORF1ab target region) copies per 20  $\mu\text{L}$  of PCR reaction mixture (or 10  $\mu\text{L}$  of RNA sample). The dynamic range is 4 to 100 copies and the assay time is less than 1.5 h.

## METHODOLOGY

**Droplet Digital PCR.** A typical 20  $\mu\text{L}$  reaction mixture was prepared by mixing 5  $\mu\text{L}$  of Master Mix (4 $\times$ , Thermo Scientific TaqPath 1-Step Multiplex Master Mix), 1  $\mu\text{L}$  of 2019-nCoV assay (20 $\times$ , Thermo Scientific TaqMan 2019nCoV Assay Kit v1), 2  $\mu\text{L}$  of 20 wt % Pluronic F127 (Sigma-Aldrich, BioReagent) aqueous solution, 10  $\mu\text{L}$  of template sample, and 2  $\mu\text{L}$  of nuclease-free water. The 1  $\mu\text{L}$  of 2019-nCoV reverse-transcription PCR assay consisted of N primers/probe set or ORF1ab primers/probe set. The volumes of Pluronic F127 solution, template sample, and nuclease-free water could be adjusted according to template concentration and droplet size for optimum efficiency and stability. After reaction mixtures preparation, the mixtures were generated into droplets in 200  $\mu\text{L}$  PCR tubes as described below. Then the PCR tubes were placed into a thermal cycler (Bio-Rad, MJ Mini Thermal Cycler), and thermal cycling was performed at 50 °C for 5 min and 95 °C for 2 min and then 30–40 cycles of 95 °C for 3 s and 60 °C for 30 s. Including the heating/cooling times for each step, the typical times for the reaction is 55 min for 30 cycles and 70 min for 40 cycles for this thermal cycler.

**Droplet Generation.** The head part of a pipette tip (Eppendorf microloader) was flattened by pressing a piece of glass slide on top of it for 10 s. In order to maintain

consistency, manually pressed tips were prepared in batches and the tips with cross-section aspect ratios between 3.5 and 4 were utilized for droplet PCR experiments. Commercial gel-loading flat pipette tips (Axygen TGL10FT17R) were used as-bought. For droplet generation, a universal 20  $\mu\text{L}$  pipette gun was used for the head-flattened pipette tip to draw and dispense liquid. Then 10  $\mu\text{L}$  of oil (HFE 7500 3 M Novec with 1–2 wt % RAN 008 surfactant or with 2 v/v% Krytox 157 FSH) was drawn into a head-flattened tip to wet the interior of the head-flattened pipette tips. The oil was expelled out and 20  $\mu\text{L}$  of the PCR reaction mixture was drawn into the head-flattened pipette tip. Subsequently, the PCR reaction mixture was pipetted out manually into 50  $\mu\text{L}$  of oil in a 200  $\mu\text{L}$  PCR tube. At typical pipette dispensing flow rates, the droplet size was insensitive to minor shaking and flow rate variations caused by the manual operation. Droplet size uniformity was hence quite robust. Normally, it took 3–5 min to convert 20  $\mu\text{L}$  reaction mixture into uniform droplets.

**Imaging.** After PCR thermal cycling, the droplets together with the oil in the 200  $\mu\text{L}$  tube were collected and transferred via regular round pipette tips with manual pipetting to the center of a covered frame seal (Bio-Rad, 65  $\mu\text{L}$  #SLF0601) on a glass slide. The plastic cover of the frame seal helped immobilize the droplets monolayer. The entire monolayer suspension occupied an area of about 1  $\text{cm}^2$  and hence easily fitted into visual or smartphone field of view such that one image contained all the droplets. As a reference, these droplets were imaged by a table-top fluorescence microscope (Olympus IX71) and/or a portable fluorescence mini-microscope (Dino-Lite AM4115T-GFBW). For smartphone camera imaging or visual counting, the glass slide with droplets was placed onto a transilluminator (Clare Chemical Research), and the blue light illuminated droplets in dark or dim ambient environment were recorded by the camera of an OnePlus 7 Pro smartphone.

## RESULTS AND DISCUSSION

As a reference, a commercial microloading pipette tip (~200  $\mu\text{m}$  diameter orifice) was first used to generate water droplets in HFE7500 oil with 2 wt % fluorosurfactant (Figure 1a,b). The prepared water droplets were mostly around 600  $\mu\text{m}$  in diameter and the droplets show significant CV  $\approx 9.6\%$  in the droplet size (Figure 1c). After the head of the tip was flattened into an elliptical shape with an aspect ratio of about 4, larger than the theoretical limit of 3.5 for monodispersed droplets, uniform water droplets of  $157 \pm 4 \mu\text{m}$  diameter were generated with a CV of 2.3% (Figure 1e–g). The same head-flattened tip pipette generated equally monodispersed but slightly larger droplets with the more viscous PCR solution (Figure 1h,  $177 \pm 6 \mu\text{m}$  diameter due to the viscosity difference, CV 3.1%) while the as-bought tip totally failed (Figure 1d). Multiple droplet generation trials with head-flattened pipette tips of various cross-section aspect ratios were conducted. Uniform droplets were produced with aspect ratios over 3.5. Higher aspect ratios would produce smaller and more uniform droplets (Figure S1). Like their microfluidic chip counterparts, the size and monodispersity of the droplets generated by the flattened elliptical pipette tip were insensitive to the flow rate so that it was possible to generate uniform droplets just by pushing a regular pipette gun equipped with a head-flattened tip. Usually, 3–5 min completed the entire ~5000 droplet generation process from 20  $\mu\text{L}$  of the PCR reaction mixture directly into a 200  $\mu\text{L}$  PCR tube loaded with 50  $\mu\text{L}$  of oil, corresponding to a droplet generation rate of

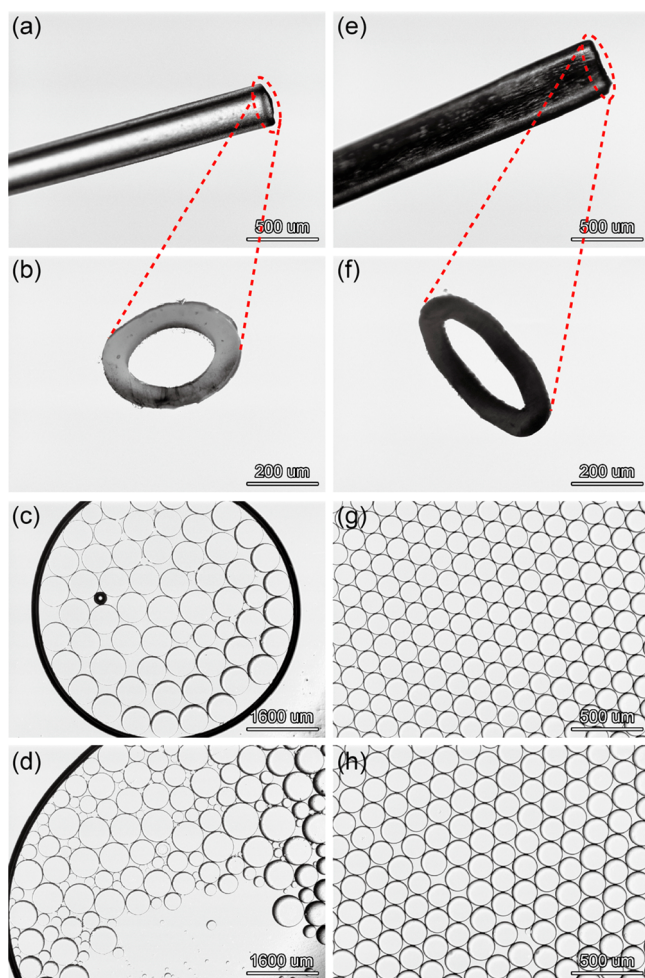


**Figure 1.** Droplets generation with pipette tips: (a, b) the top-view and cross-section of the commercial microloading pipette tip, the generated (c) water droplets and (d) PCR reaction mixture droplets; (e, f) the top-view and cross-section of the pipette tip with flattened head and the generated (g) water droplets and (h) PCR reaction mixture droplets.

about 30 Hz (Movie S1). This was slow compared to commercial droplet generation technologies, but we had (100 $\times$ ) fewer droplets to generate. There was almost no reaction mixture loss (all mixture were drawn into the pipette tip and then pipetted out completely into oil in the droplets) from droplet generation and the as-generated droplets in the PCR tubes were ready to be put into a thermal cycler for PCR reaction. Pipette droplet generation right into PCR tubes is hence an effective way to prepare monodispersed large microdroplets for ddPCR.

Now that uniform large microdroplets could be prepared by head-flattened tips with a pipette gun, the next step was to confirm the effectiveness of the PCR reaction in the droplets. Unfortunately, after 40 PCR thermal cycles, the large microdroplets of the reaction mixture coalesced severely (Figure 2a, left). The commercial fluorosurfactant consisted of poly(ethylene glycol) and perfluoropolyethers (PFPE) blocks could not stabilize droplets of  $\sim 100 \mu\text{m}$  diameter for the PCR reaction<sup>21</sup> and would fare even worse for our larger ( $> 150 \mu\text{m}$ ) droplets. To solve this problem, polyoxyalkylene block copolymer F127 solution was introduced into the PCR reaction mixture to stabilize the droplets from inside. The

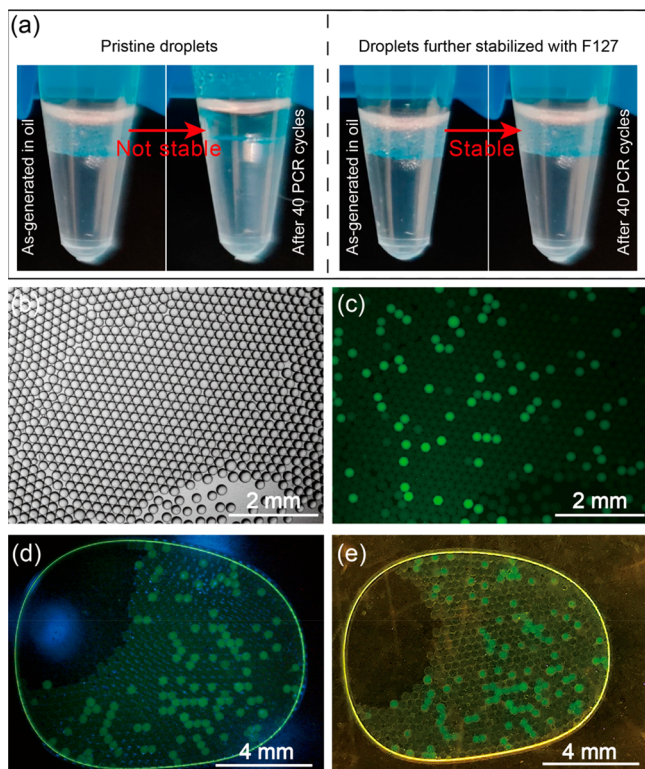


**Figure 2.** Efficient ddPCR with stabilized large microdroplets: (a) larger microdroplets are stable for PCR thermal cycling when stabilized by block copolymer F127 ( $\geq 0.01$  w/v%), (b, c) stabilized droplets after 40 PCR cycles as imaged by table-top fluorescence microscope, (d, e) identical droplets imaged by hand-held fluorescence mini-microscope and smartphone camera with a transilluminator. The stabilized large droplets are perfect for ddPCR and an appropriate large size could enable visual or smartphone camera inspection of positive droplets.

F127 three-block copolymer was chosen because it contained the poly(ethylene oxide) (PEO) blocks which was the hydrophilic segments of the surfactant in the oil.<sup>29</sup> Another reason was that the F127 solution could respond to high temperatures with versatile micelle formation and aggregation/patterning which was the mechanism for the gelation of F127 solution at elevated temperatures.<sup>27,28</sup> Moreover, the poly-oxyalkylene chemistry of F127 was benign to the PCR reaction.<sup>30,31</sup> With over 0.01 w/v% of F127 in the PCR reaction mixture, the large microdroplets could withstand 40 PCR thermal cycles without droplet coalescence (Figure 2a, right). The stabilization of aqueous droplets by F127 in fluorocarbon oil was further confirmed by generating droplets in HFE7500 oil with 2 v/v% Krytox 157 FSH (Figure S2). With over 0.01 w/v% F127 in water, uniform aqueous droplets were produced. Otherwise, the droplets would coalesce right after pipette generation.

After stabilizing the large droplets for PCR thermal cycling, we established that large droplets in the 150–350  $\mu\text{m}$  range can produce visually or smartphone detectable droplets with a transilluminator. As a benchmark, both a table-top commercial fluorescence microscope (Figure 2b,c) and a hand-held fluorescence microscope were also used (Figure 2d). All images by different detectors allow easy identification of positive lit droplets (Figure 2c–e). Because the droplets were over 150  $\mu\text{m}$ , positive droplets could also be discerned by the human eye within a distance of 50 cm, when illuminated by a

universal filtered transilluminator with blue light in a dark or dim ambient environment. Hence, a smartphone camera or even the naked human eye were able to record the positive droplets with good fidelity (Figure 2e). The hand-held microscope had better resolution than the smartphone camera images (Figure 2d) for the same droplet suspension, but the positive droplets are completely discernible in the smartphone camera image.

The resolution by visual detection was scrutinized. A series of 20  $\mu\text{L}$  PCR reaction mixtures were prepared with nominally 2, 10, 25, 50, and 100 copies of template and two target regions (N, ORF1ab) were detected, respectively. In Figure 3, we showed the hand-held mini-microscope and smartphone images of the samples, each with 20  $\mu\text{L}$  of PCR reaction. The smartphone camera images had identical numbers of lit droplets to mini-microscope images, and the numbers were close to the nominal values. For small copy number samples with 2, 10, 25, and 50 copies of target, droplets used were around 300  $\mu\text{m}$  generated by head-flattened tips with cross-section aspect ratios slightly larger than 3.5, for better visual detection after PCR reaction. This larger droplet size produced about 1500 droplets from 20  $\mu\text{L}$  of the reaction mixture. It was a large enough droplet number relative to the copy number (larger than a factor of  $\sim 30$ ) to ensure no more than one target per droplet so that quantification could be done by counting only the lit positive droplets. In addition, droplets around 300  $\mu\text{m}$  could also be produced by commercial gel-loading flat pipette tips for droplet digital PCR tests (Figure S3). For the higher copy number samples with nominally 100 target copies (Figure 3i,j), more droplets were required, and we generated about 5000 200- $\mu\text{m}$  droplets from 20  $\mu\text{L}$  of the reaction mixture with a tip cross-section aspect ratio close to 4 to guarantee Poisson distribution of one target per positive droplet. Repeated experiments (over 5 times for each sample point) were conducted for both N and ORF1ab target sequences (Figure 4, error bars are standard deviations). If the regression method with a 95% confidence interval was used to analyze the data in Figure 4,<sup>32</sup> the estimated LoDs were 3.8 (N target sequence) and 3.0 (ORF1ab target sequence) copies per 20  $\mu\text{L}$  of the reaction (Figure S4). If mean values and standard deviations of blank samples and low concentration samples were used,<sup>33</sup> the calculated LoDs were 2.2 (N target sequence) and 2.5 (ORF1ab target sequence) copies per 20  $\mu\text{L}$  of reaction (Table S1). Both estimates were hence comparable and consistent with reported values for commercial ddPCR with expensive optics. From the blank sample data in Table S1, contamination and primer dimerization were a source of error at low copy number. Other larger sources of error were, however, analyte loss during pipette handling and sample dilution at low target number and insufficient droplet number at large copy number (approaching 100) to ensure a single copy per positive droplet (from the growing standard deviation with respect to copy number in Figure 4).

Moreover, we confirmed that our 150–350  $\mu\text{m}$  droplets allow quantification after a typical 30–40 cycle amplification. Reactions with no template or 10 copies of template in 20  $\mu\text{L}$  of the mixture were done in bulk and in droplets. After cycling, the bulk mixture was converted into droplets for fluorescence intensity comparison. All samples for intensity comparison were imaged (table-top fluorescence microscope) and analyzed (ImageJ) under the same conditions. The normalized fluorescence intensity differences from bulk PCR samples with 0 or 10 target copies (Figure 5a,c) and from positive and

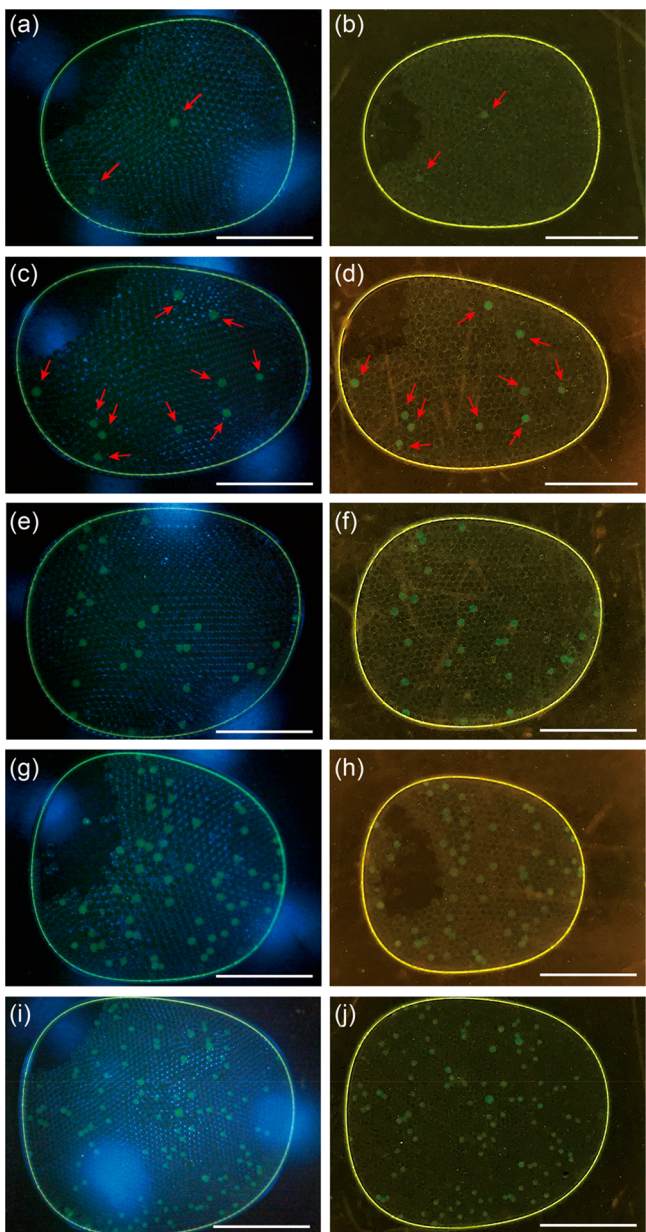


**Figure 3.** POC ddPCR of low target copy samples: (a, c, e, g, and i) hand-held fluorescence mini-microscope images of samples with nominally 2, 10, 25, 50, and 100 template copies in 20  $\mu\text{L}$  of the PCR reaction mixture, respectively; (b, d, f, h, and j) smartphone camera images of samples with nominally 2, 10, 25, 50, and 100 template copies in 20  $\mu\text{L}$  of the PCR reaction mixture, respectively. Large microdroplets could be imaged by smartphone, and the outcomes are consistent with those of a hand-held fluorescence mini-microscope. The scale bars are 4 mm.

negative droplets of droplet PCR (Figure 5b,d) showed that the PCR reaction done in droplets had better contrast, by 21 times at the threshold of 30 cycles when the bulk intensity could not be discerned (Figure 5e). In general, 30 to 40 cycles were sufficient to allow detection of positive droplets with single molecules by eye or by smartphone imaging (Figure S5). These were high but feasible cycle numbers that could be achieved with the usual PCR mixture.

Finally, we demonstrated the possibility of using large droplets for RNA-extraction-free detection. Bulk rt-PCR tests of SARS-CoV-2 nasopharyngeal/sputum/saliva samples with-

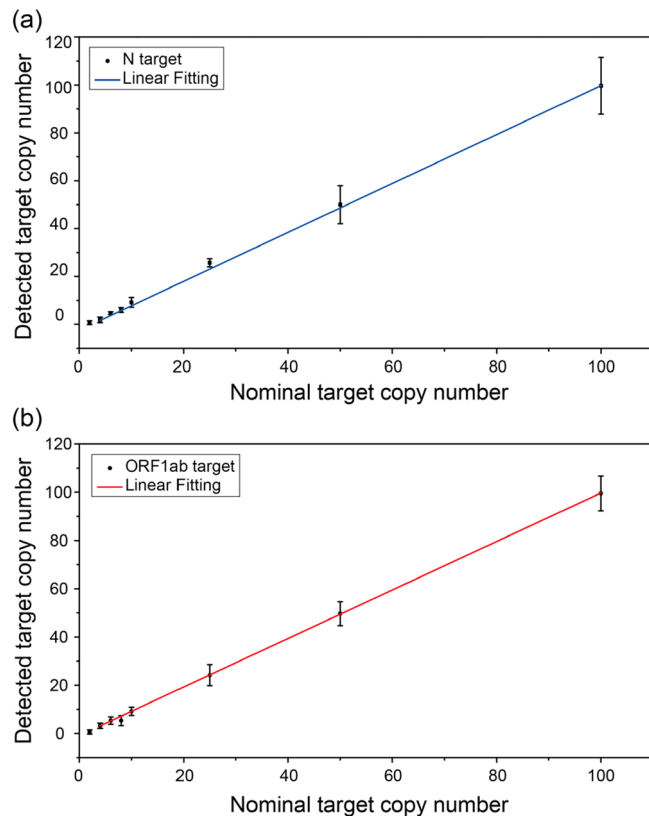


**Figure 4.** Detected numbers of targets by counting all positive droplets: (a) detection of the N target region and (b) detection of the ORF1ab target region.

out RNA extraction have been reported<sup>34–37</sup> and it would be interesting to see if this step could be avoided for the current ddPCR platform. Uninfected raw saliva was added to the reaction mixture for droplet generation and PCR reaction. Because saliva changes the sample surface tension and viscosity, the droplets containing saliva were larger (Figure 6). No copy was detected from a 10-copy sample with 20 v/v% saliva, which also showed polydispersed droplet size. Nevertheless, for nominally 10 target copies,  $9.6 \pm 2.1$  and  $8.7 \pm 2.5$  (mean and standard deviation from 5 tests) positive droplets were observed for saliva-free and 10 v/v% saliva-doped samples, respectively. The difference was roughly consistent with errors due to target concentration fluctuation in Figure 4, suggesting that PCR-inhibition from saliva samples can be eliminated with moderate dilution (Figure 6d). Therefore, without testing a large number of samples, ddPCR showed promise for low viral load detection without RNA extraction from slightly diluted saliva samples.

## CONCLUSION

Uniform large microdroplets with diameters from 150 to 350  $\mu\text{m}$  are generated by a regular pipette gun equipped with head-flattened pipette tips, in place of the bulky and delicate micropumps for smaller droplet generation. A polyoxyalkylene block copolymer F127 surfactant is utilized to further stabilize these large droplets for robust PCR thermal cycling. The droplets have demonstrated good efficiency for ddPCR, and the probable total assay time is about 1.5 h including 10 min for sample preparation (commercial RNA extraction kits or RNA-extraction-free), 5 min for droplet generation, 5 min for reverse transcription plus 60 min for 40 thermal cycles, and 5

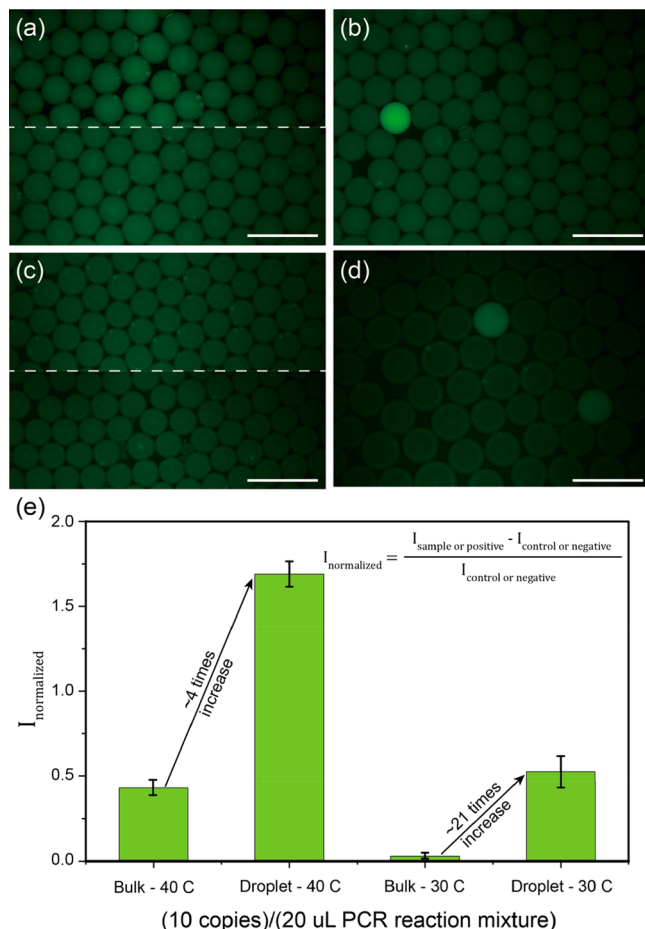


**Figure 5.** Fluorescence intensity comparison between bulk PCR and droplet PCR: (a) droplets generated after 40 cycles of bulk PCR with 10 target copies (top) and 0 target copy (bottom); (b) droplets from 40 cycles droplet PCR with 10 target copies; (c) droplets generated after 30 cycles of bulk PCR with 10 target copies (top) and 0 target copies (bottom); (d) droplets from 30 cycles droplet PCR with 10 target copies; (e) normalized fluorescence intensity comparison between bulk and droplet PCR. The scale bars are 500  $\mu\text{m}$ .

min for droplet spreading and visual inspection. Reduction of assay time to 1 h or even 45 min is quite feasible with more expensive or specially designed thermal cyclers. With rapid (10 min) isothermal amplification like recombinase polymerase amplification, a sub-30 min assay would be possible.<sup>38</sup> Thanks to the large size and also still significant reporter concentration, the droplets can be detected and, for small copy number, counted visually. It hence does not require any optical detector for low copy numbers, which is another major obstacle for POC applications. The LODs of 3.8 copies per 20  $\mu\text{L}$  of reaction are as good as any commercial lab-bound optical PCR platform, bulk or digital. Our technology hence satisfies all of the necessary features for a rapid POC ddPCR test. Its thousands of droplets can allow a sufficiently large dynamic range of 4–100 copies that is still within the Poisson limit of a single molecule per droplet. For quantification of a large copy number, it is better to utilize diluted samples to ensure accurate quantification and easy counting.

Our low-viral load POC test can also be used for other infectious viral and bacterial diseases. Though it may be possible to conduct POC ddPCR tests without RNA extraction for saliva samples, purified samples would still permit more

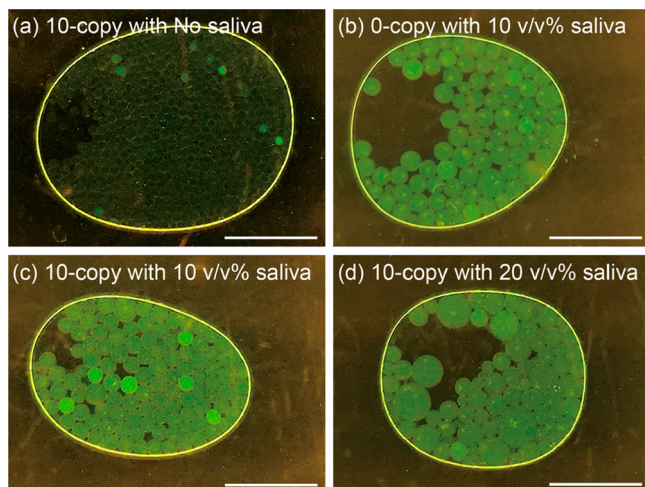


**Figure 6.** POC ddPCR of (a) saliva-free sample with nominally 10 target copies, (b) 10 v/v% saliva-doped sample with no target molecule, (c) 10 v/v% saliva-doped sample with nominally 10 target copies, and (d) 20 v/v% saliva-doped sample with nominally 10 target copies showing polydispersed droplets and no positive droplets. The tolerance of moderate saliva impurities indicates that POC ddPCR is possible for some RNA-extraction-free tests. The images are from a smartphone camera, and the scale bars are 4 mm.

precise quantification and reduction of false negatives, particularly for more heterogeneous samples like blood or nasopharyngeal samples. Commercial kits are available for RNA extraction, but they may not extract the RNA at high yield or from large sample volume efficiently.<sup>39</sup> Given the tremendous advantages of our new downstream droplet generation and visual detection platform, a different paradigm for upstream pretreatment may be in order. One that can filter the original sample, say the VTM sample, down to 10  $\mu\text{L}$  without virus loss would further enhance the sensitivity of the integrated platform to complement the rapidity and portability of the current POC detection platform.

## ASSOCIATED CONTENT

### Supporting Information

The Supporting Information is available free of charge at <https://pubs.acs.org/doi/10.1021/acs.analchem.1c00192>.

Pipette droplet generation with head-flattened tips ([MP4](#))

Additional supporting material as discussed in the text including Figures S1–S5 and Table S1 ([PDF](#))

## AUTHOR INFORMATION

### Corresponding Author

Hsueh-Chia Chang – Department of Chemical and Biomolecular Engineering, University of Notre Dame, Notre Dame, Indiana 46556, United States; Email: [hchang@nd.edu](mailto:hchang@nd.edu)

### Authors

Liao Chen – Department of Chemical and Biomolecular Engineering, University of Notre Dame, Notre Dame, Indiana 46556, United States; [orcid.org/0000-0001-8294-6892](https://orcid.org/0000-0001-8294-6892)

Vivek Yadav – Department of Chemical and Biomolecular Engineering, University of Notre Dame, Notre Dame, Indiana 46556, United States

**Chenguang Zhang** – Department of Chemical and Biomolecular Engineering, University of Notre Dame, Notre Dame, Indiana 46556, United States

**Xiaoye Huo** – Department of Chemical and Biomolecular Engineering, University of Notre Dame, Notre Dame, Indiana 46556, United States

**Ceming Wang** – Department of Chemical and Biomolecular Engineering, University of Notre Dame, Notre Dame, Indiana 46556, United States;  [orcid.org/0000-0002-1328-6410](https://orcid.org/0000-0002-1328-6410)

**Satyajyoti Senapati** – Department of Chemical and Biomolecular Engineering, University of Notre Dame, Notre Dame, Indiana 46556, United States

Complete contact information is available at:  
<https://pubs.acs.org/10.1021/acs.analchem.1c00192>

## Author Contributions

L.C. designed, engineered, and optimized the technology. H.-C.C. initiated and managed the project. V.Y. contributed to the droplet generation effort. C.Z., X.H., and C.W. assisted with the testing and imaging. L.C. and H.-C.C. wrote the paper with contributions from all authors.

## Notes

The authors declare no competing financial interest.

## ACKNOWLEDGMENTS

This work has been supported by the NIH Common Fund, through the Office of Strategic Coordination/Office of the NIH Director, 1UG3CA241684-01, by the Institute for Precision Health at University of Notre Dame and by a generous gift from Thomas Hedrick.

## REFERENCES

- (1) Arnaout, R.; Lee, R. A.; Lee, G. R.; Callahan, C.; Yen, C. F.; Smith, K. P.; Arora, R.; Kirby. *J. E. bioRxiv* **2020**, DOI: 10.1101/2020.06.02.131144.
- (2) Kucirka, L. M.; Laufer, S. A.; Laeyendecker, O.; Boon, D.; Lessler. *Ann. Intern. Med.* **2020**, 173, 262–268.
- (3) Xiao, A. T.; Tong, Y. X.; Zhang, S. *J. Med. Virol.* **2020**, 92, 1755–1756.
- (4) Feng, W.; Newbigging, A. M.; Le, C.; Pang, B.; Peng, H.; Cao, Y.; Wu, J.; Abbas, G.; Song, J.; Wang, D.-B.; Cui, M.; Tao, J.; Tyrrell, D. L.; Zhang, X.-E.; Zhang, H.; Le, X. C. *Anal. Chem.* **2020**, 92, 10196–10209.
- (5) Hindson, C. M.; Chevillet, J. R.; Briggs, H. A.; Gallichotte, E. N.; Ruf, I. K.; Hindson, B. J.; Vessella, R. L.; Tewari, M. *Nat. Methods* **2013**, 10, 1003–1005.
- (6) Suo, T.; Liu, X.; Feng, J.; Guo, M.; Hu, W.; Guo, D.; Ullah, H.; Yang, Y.; Zhang, Q.; Wang, X.; Sajid, M.; Huang, Z.; Deng, L.; Chen, T.; Liu, F.; Xu, K.; Liu, Y.; Zhang, Q.; Liu, Y.; Xiong, Y.; et al. *Emerging Microbes Infect.* **2020**, 9, 1259–1268.
- (7) Alteri, C.; Cento, V.; Antonello, M.; Colagrossi, L.; Merli, M.; Ughi, N.; Renica, S.; Matarazzo, E.; Di Ruscio, F.; Tartaglione, L.; Colombo, J.; Grimaldi, C.; Carta, S.; Nava, A.; Costabile, V.; Baiguera, C.; Campisi, D.; Fanti, D.; Vismara, C.; Fumagalli, R.; et al. *PLoS One* **2020**, 15, e0236311.
- (8) Falzone, L.; Musso, N.; Gattuso, G.; Bongiorno, D.; Palermo, C. I.; Scalia, G.; Libra, M.; Stefani, S. *Int. J. Mol. Med.* **2020**, 46, 957–964.
- (9) Sanders, R.; Mason, D. J.; Foy, C. A.; Huggett, J. F. *PLoS One* **2013**, 8, e75296.
- (10) Mello, C. J.; Kamitaki, N.; de Rivera, H.; McCarroll, S. A. *medRxiv* **2020**.
- (11) Pan, Z.; Men, Y.; Senapati, S.; Chang, H.-C. *Biomicrofluidics* **2018**, 12, 044113.
- (12) Yin, J.; Hu, J.; Sun, J.; Wang, B.; Mu, Y. *Analyst* **2019**, 144, 7032–7040.
- (13) Chen, Z.; Liao, P.; Zhang, F.; Jiang, M.; Zhu, Y.; Huang, Y. *Lab Chip* **2017**, 17, 235–240.
- (14) Pinheiro, L. B.; Coleman, V. A.; Hindson, C. M.; Herrmann, J.; Hindson, B. J.; Bhat, S.; Emslie, K. R. *Anal. Chem.* **2012**, 84, 1003–1011.
- (15) Basu, A. S. *Slas. Technol.* **2017**, 22, 369–386.
- (16) Hindson, B. J.; Ness, K. D.; Masquelier, D. A.; Belgrader, P.; Heredia, N. J.; Makarewicz, A. J.; Bright, I. J.; Lucero, M. Y.; Hiddessen, A. L.; Legler, T. C.; Kitano, T. K.; Hodel, M. R.; Petersen, J. F.; Wyatt, P. W.; Steenblock, E. R.; Shah, P. H.; Bousse, L. J.; Troup, C. B.; Mellen, J. C.; Wittmann, D. K.; et al. *Anal. Chem.* **2011**, 83, 8604–8610.
- (17) Xu, X. N.; Yuan, H. J.; Song, R. Y.; Yu, M.; Chung, H. Y.; Hou, Y. M.; Shang, Y. H.; Zhou, H. B.; Yao, S. H. *Biomicrofluidics* **2018**, 12, 014103–014110.
- (18) Dangla, R.; Kayi, S. C.; Baroud, C. N. *Proc. Natl. Acad. Sci. U. S. A.* **2013**, 110, 853–858.
- (19) Dutka, F.; Opalski, A. S.; Garstecki, P. *Lab Chip* **2016**, 16, 2044–2049.
- (20) Mei, L. P.; Jin, M. L.; Xie, S. T.; Yan, Z. B.; Wang, X.; Zhou, G. F.; van den Berg, A.; Shui, L. L. *Lab Chip* **2018**, 18, 2806–2815.
- (21) Montessori, A.; Lauricella, M.; Succi, S.; Stolovicki, E.; Weitz, D. *Phys. Rev. Fluids* **2018**, 3, 072202.
- (22) Li, H. T.; Wang, H. F.; Wang, Y.; Pan, J. Z.; Fang, Q. *Talanta* **2020**, 217, 217.
- (23) Chowdhury, M. S.; Zheng, W. S.; Kumari, S.; Heyman, J.; Zhang, X. C.; Dey, P.; Weitz, D. A.; Haag, R. *Nat. Commun.* **2019**, 10, 10.
- (24) Yin, K.; Zeng, X.; Liu, W.; Xue, Y.; Li, X.; Wang, W.; Song, Y.; Zhu, Z.; Yang, C. *Anal. Chem.* **2019**, 91, 6003–6011.
- (25) Zhu, Y.; Li, J.; Lin, X.; Huang, X.; Hoffmann, M. R. *bioRxiv* **2019**, 848168.
- (26) Alexandridis, P.; Alan Hatton, T *Colloids Surf, A* **1995**, 96, 1–46.
- (27) Mortensen, K.; Pedersen, J. S. *Macromolecules* **1993**, 26, 805–812.
- (28) Wanka, G.; Hoffmann, H.; Ulbricht, W. *Macromolecules* **1994**, 27, 4145–4159.
- (29) Holtze, C.; Rowat, A. C.; Agresti, J. J.; Hutchison, J. B.; Angile, F. E.; Schmitz, C. H. J.; Koster, S.; Duan, H.; Humphry, K. J.; Scanga, R. A.; Johnson, J. S.; Pisignano, D.; Weitz, D. A. *Lab Chip* **2008**, 8, 1632–1639.
- (30) Kuan, I.; Gu, W. G.; Wu, J. C.; Wei, C. H.; Chen, K. S.; Yu, C. Y. *Chem. Eng. J.* **2008**, 143, 326–330.
- (31) Schrader, C.; Schielke, A.; Ellerbroek, L.; Johne, R. *J. Appl. Microbiol.* **2012**, 113, 1014–1026.
- (32) Christian, G. D.; Dasgupta, P. K.; Schug, K. A. *Analytical Chemistry*, 7th ed.; Wiley, 2013; Chapter 3, p 107.
- (33) Armbruster, D. A.; Pry, T. *Clin. Biochem. Rev.* **2008**, 29, S49–S52.
- (34) Smyrlaki, I.; Ekman, M.; Lentini, A.; Rufino de Sousa, N.; Papanicolau, N.; Vondracek, M.; Aarum, J.; Safari, H.; Muradrasoli, S.; Rothfuchs, A. G.; Albert, J.; Höglberg, B.; Reinius, B. *Nat. Commun.* **2020**, 11, 4812.
- (35) Wee, S. K.; Sivalingam, S. P.; Yap, E. P. H. *bioRxiv* **2020**, 2020.2004.2017.042366.
- (36) Miranda, J. P.; Osorio, J.; Videla, M.; Angel, G.; Camponovo, R.; Henriquez-Henriquez, M. *Front. Med.* **2020**, 7, 7.
- (37) Fukumoto, T.; Iwasaki, S.; Fujisawa, S.; Hayasaka, K.; Sato, K.; Oguri, S.; Taki, K.; Nakakubo, S.; Kamada, K.; Yamashita, Y.; Konno, S.; Nishida, M.; Sugita, J.; Teshima, T. *Int. J. Infect. Dis.* **2020**, 98, 16–17.
- (38) Xia, S.; Chen, X. *Cell Discovery* **2020**, 6, 37.
- (39) Zhang, C.; Sun, G.; Senapati, S.; Chang, H.-C. *Lab Chip* **2019**, 19, 3853–3861.